Metallurgy and Foundry Engineering – Vol. 41, 2015, No. 1, pp. 29–44
http://dx.doi.org/10.7494/mafe.2015.41.1.29

Paweł Hyjek, Iwona Sulima, Piotr Malczewski

Mechanical properties and corrosion resistance of cast NiAl alloys with the addition of Ti

Własności mechaniczne oraz odporność na korozję stopów NiAl z dodatkiem tytanu

Abstract
Results of compression- and corrosion-resistance tests of NiAl alloys with 1.0 and 2.0 wt.% of titanium are described. The compression tests conducted at a wide range of temperatures, and the strain rate showed that an increase in titanium content causes increased brittleness at room temperature, while at higher temperatures, an increase of hardness and strength is observed. The analysis of electrochemical corrosion resistance showed that alloys containing Ti are characterized by considerable resistance to sulfuric acid VI, because the emerging titanium oxide prevents the active solubilization of the alloy. Besides, microstructure observations performed at various levels of deformation, which allowed us to identify the mechanisms responsible for fracture of the studied alloys.

Keywords: NiAl alloys, compression, corrosion resistance

Streszczenie
W artykule zamieszczono wyniki badań wytrzymałości i odporności na korozję stopów na osnowie fazy NiAl z dodatkiem 1.0 i 2.0% wag. tytanu. Prowadzone w szerokim zakresie temperatur i prędkości odkształcania próby ściskania wykazały, że wzrost zawartości tytanu wpływa na zwiększenie kruchości stopu w temperaturze pokojowej, podczas gdy w podwyższonych temperaturach obserwuje się zwiększenie twardości i wytrzymałości. Analiza odporności na korozję elektrochemiczną ujawniła, że stopy zawierające tytan charakteryzują się znaczą odpornością na działanie kwasu siarkowego VI, bowiem powstający tlenek tytanu utrudnia aktywne roztwarzanie stopu. Wykonano także obserwacje mikrostrukturalne na różnych poziomach odkształcenia, które pozwoliły na identyfikację mechanizmów odpowiedzialnych za zniszczenie (pękanie) stopów.

Słowa kluczowe: stopy NiAl, ściskanie, odporność korozyjna

Paweł Hyjek Ph.D. Eng., Iwona Sulima Ph.D. Eng., Piotr Malczewski Ph.D. Eng.: Institute of Technology, Pedagogical University of Cracow; phyjek@up.krakow.pl

1. Introduction

Due to outstanding physic-chemical and mechanical properties, alloys with a matrix made of intermetallic phases containing aluminum belong to a group of materials operating at higher temperatures in a corrosive environment. Unique features of NiAl-based alloys include: low density, high melting temperature, good hardness, Young modulus and thermal conductivity as well as sufficient corrosion resistance. This choice of properties makes these alloys suitable for elements of gas turbines, combustion engines, heat exchangers and engines working at high temperatures and in a corrosive environment. The range of applications of these alloys is limited by insufficient ductility and resistance to cracking at ambient temperatures, as well as by their poor resistance to cracking at higher temperatures [1–5].

In order to extend the spectrum of applications of NiAl matrix alloys, studies regarding the improvement of mechanical properties are undertaken, mainly an increase of plasticity at room temperature by micro and macro alloying additions [3–6]. It was observed that, in the case of a single phase NiAl alloy with a B2 phase, there is a possibility of a significant control of brittleness. The generation of monocrystalline or fine policrystalline phase considerably increased ductility at higher temperatures. Still, attempts have been made towards decreasing brittleness at room temperature.

Until now, it has been shown that the addition of Cu, Fe, Ag, Co and Ti [7, 8] in the form of modifiers of single or binary phase structure significantly improves the mechanical properties of the intermetallic NiAl phase. Another solution for increasing the strength of NiAl alloys is the introduction of hard, fine ceramic particles that are metallurgically stable at higher temperatures [6, 9, 10].

Simultaneously to studies regarding mechanical properties of NiAl-based alloys, investigations were conducting towards determining corrosion resistance. The basic method of studying electrochemical properties of metals and alloys (passivation) is the determination of anodic or cathodic polarization curves. The dependence of density on an external polarization current flowing thorough a sample of potential U is measured at potentiostat with respect to a reference electrode. The obtained characteristics allow us to determine anodic behavior of a given alloy in certain environments. Besides, it is also possible to prepare and hold an alloy in a passive state as well as determine the influence of temperature and environment changes on a course of electrode processes and influence of corrosion inhibitors [11]. The advancing chemical or electrochemical corrosion may cause a considerable decrease of mechanical and tribological properties as well as economic losses due to damage to the materials.

It is to note that, in metallic alloys, structural parameters other than electrochemical ones strongly affect the intensity of corrosion. A condition for intensive electrochemical corrosion in alloys is the formation of galvanic microcells caused by the presence of at least two phases in the microstructure. Thus, the basic elements of microcells are secondary precipitates or metallic impurities present in a matrix (mainly at grain boundaries).

Moreover, energetic parameters connected with grain-size and internal stresses influence the intensity of the electrochemical corrosion; usually, the smaller the grain, the less corrosion. Although, many things were achieved in the understanding and description of this type of destruction process of metals and alloys, many experiments are still required [12].

2. Materials and experimental method

2.1. Obtaining alloys

Smelting techniques of intermetallic phases include: smelting in an open-induction furnace, smelting in a vacuum, induction remelting in a vacuum, and smelting in an arc furnace. The smelting process of intermetallic phase NiAl must be carried out under specific conditions due to the large difference in melting temperatures of pure aluminum (933 K) and nickel (1728 K), and the presence of an exothermic reaction occurring during synthesis (which is not insignificant for the metallurgic process). Due to the rapid increase in temperature immediately after an exothermic reaction, oxidation of aluminum in air takes place, which causes the formation of slag. Thus, precise control of an alloy's composition is rendered difficult.

The alloys for studies were produced in the Exomelt cost-saving process in a protective argon atmosphere at subatmospheric pressure of 0.5 MPa. The procedure of placing a charge material in equipment is described in [13]. The time necessary for reaching a pouring temperature was 500 s. For comparison, in a classic method, the time for reaching the melting temperature of pure nickel (when aluminum could be added) is 820 s. Therefore, saving of energy in the case of the modified Exomelt technique is 40%. The exothermic reaction of Ni-Al lasts a few seconds; then, the alloy can be poured by classic methods to a heated mould. The described method was applied for receiving NiAl with Ti and B additions. Boron was added in the form of master alloy Al-3%B after the exothermic reaction was finished.

The obtained alloys were poured to a multiple mould in an argon atmosphere, allowing for the receipt of four ingots with different dimensions depending on the destination of the samples. From the obtained rods, samples were cut by a spark-erosion cutting device for compression and Vickers hardness tests, and a series of specimens were cut for corrosion-resistance experiments.

2.2. Experimental methods

In order to control chemical and phase composition, alloys were subjected to X-ray analysis by a DRON-s diffractometer equipped with a copper tube with an LiF monochromator. Measurements were performed for 2θ in the range 20–120° at an exposure time of 6 s and a step size of 0.02°. The working voltage and current of the diffractometer were 42 kV and 18 mA, respectively.

Mechanical properties of NiAlTiB (A and B), where A and B correspond to various amounts of alloying additions, were evaluated on the basis of a compression test conducted at a wide range of temperatures and strain rates. The tests were carried out by an Instron universal machine equipped with a furnace with a dynamic-flow argon atmosphere. Samples with a diameter of 6 ± 0.03 mm and a height of 9 ± 0.05 mm were deformed at temperatures of 297, 673, 873, and 1073 K, with strain rates of $9.25 \cdot 10^{-5}\,s^{-1}$, $1.85 \cdot 10^{-4}\,s^{-1}$, and $1.85 \cdot 10^{-3}\,s^{-1}$. Prior to a test, the furnace temperature was stabilized at the required level, and each sample was held for 5 minutes before the test began to assure that there was no temperature gradient across the specimen.

Dependencies based on the concept of initial deformation proposed by Krupkowski [14] or Swift, or dependence based on the initial stress proposed by Ludwig ($\sigma = \sigma_o + Ke^n$) and modified by Hollomon ($\sigma = Ke^n$) and later by Ludwigson ($\sigma = Ke^n \pm \Delta$) are most often applied to the description of the deformation characteristics (σ-ε) [15]. It was observed in many metals and alloys that the characteristics (σ-ε) in double-logarythmic co-ordinate system $\log\sigma = f(\log\varepsilon)$ shows deviations form a linearity, especially in the case of small strains.

Structure evolution during deformation was evaluated based on the microstructural observation of metallographic samples at optical microscope Olympus GX-51 and scanning electron microscope JEOL JSM 6460 LV and PHILIPS 535 M with EDAX system for chemical analysis. The samples were etched with 45% CH_3COOH, 35% HNO_3, 10% HCl, and 10% H_3PO_4 to reveal grain boundaries. Observations of fracture surfaces were also performed.

Corrosion-resistance tests of NiAlTiB alloys were conducted in 1-mol solution of H_2SO_4. Polarization curves were obtained by cyclic voltammetry in a classic three-electrode system vented with argon. Venting the solution of sulfuric acid with argon causes the removal of oxygen; thus, the dominating cathodic reaction in an acidic solution is the reduction of hydrogen ions. Taking advantage of voltammetric curves, the following parameters can be established: passivation potential, passivation current and current of solubilizing, which are all responsible for the corrosion resistance of an alloy.

In an electrochemical vessel, a platinum net (antielectrode), working electrode (a sample), and an Ag/AgCl electrode (reference electrode) were placed. The rate of potential change for voltamperometric characeristics was 1V/min.

3. Results and discussion

3.1. Structure and mechanical properties of NiAlTiB alloys

The chemical composition of the studied alloys determined by a scanning electron microscope with EDS is presented in Table 1, while the microstructure micrograph in its initial state are presented in Figure 1.

Table 1. Chemical composition of the studied alloys

Alloy	Content of alloying elements [wt.%]				
	Symbol	Ni	Al	Ti	B
NiAlTiB	A	Bal.	23.0	1.0	0.05
	B	Bal.	22.0	2.0	0.05

Structure observations of the as-cast samples in the sections perpendicular to the direction of pouring melt to a mold are shown in Figure 1. Samples in initial state underwent heat treatment at 1523 K for 48 h, followed by cooling with a furnace to an ambient temperature

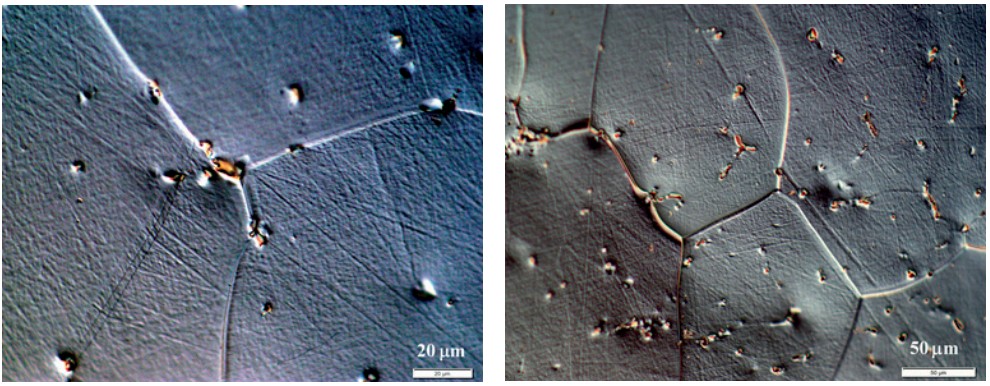

Fig. 1. Microstructures of as-cast samples, sections perpendicular to pouring direction of NiAlTiB alloys: a) A; b) B

X-ray studies allowed us to determine the spacing between planes in crystal lattice d_{hkl} basing on the Bragg's law. Experimental values of interplanar distance and intensities of the studied alloy were compared with values collected in database PDF+4 2006. Recorded diffraction patterns for both alloys prove the formation of an NiAl phase (Fig. 2).

Due to the large amount of experiments conducted, only the chosen cases of compression testing are shown in the paper in the $\sigma = f(\varepsilon)$ oraz $\log\sigma = f(\log\varepsilon)$ coordinate system. Figure 3(a–d) presents true stress-strain characteristics for A and B types of NiAlTiB alloys. Table 2 presents Vickers hardness HV10 and yield strength of alloy B. The determined coefficients of Hollomon equations for each flow curve describing ranges (K_1, K_2, n_1, n_2), and a border between these ranges ($\varepsilon_{1/2,}$ $\sigma_{1/2}$) are collected in the tables, which allows us to present their course in any coordinate system. An example of such a set of Hollomon coefficients is presented in Table 3.

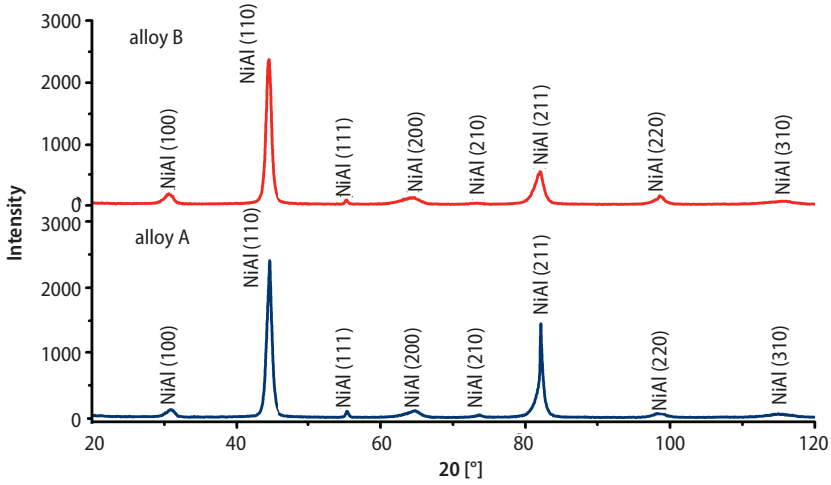

Fig. 2. Diffraction patterns of as-cast NiAlTiB alloys A and B

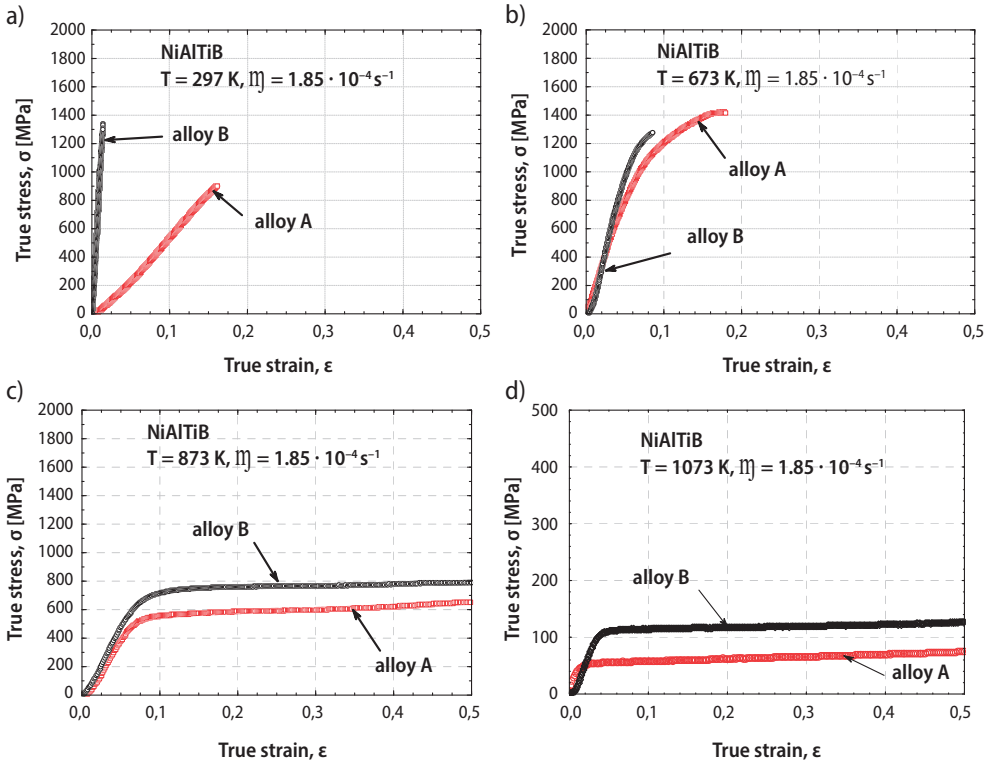

Fig. 3. Deformation characteristics of A and B types of NiAlTiB alloy at temperatures: a) 297 K; b) 673 K; c) 873 K; d) 1073 K; strain rate =1.85·10^{-4} s^{-1}

Table 2. Vickers hardness HV10 and yield points of NiAlTiB – B alloys

Alloy	Hardness HV10	Yield strength R_{02} [MPa]				
		Strain rate $\dot{\varepsilon}$ [s^{-1}]	Temperature T [K]			
			RT	673	873	1073
NiAlTiB (B)	491 ± 8.3 (1.65%)	$9.25 \cdot 10^{-5}$	1064	985	477	102
		$1.85 \cdot 10^{-4}$	1115	1034	592	125
		$1.85 \cdot 10^{-3}$	1140	835	680	142

Table 3. List of coefficients of Hollomon equation

Alloy	$\dot{\varepsilon}$ [s^{-1}] · 1.85	T [K]	K_1 [MPa]	n_1	K_2 [MPa]	n_2	$\varepsilon_{1/2}$	$\sigma_{1/2}$
NiAlTiB (A)	10^{-4}	1073	380.8027	0.4962	67.4373	0.0666	0.0178	51.5600
	10^{-3}	873	5788.9527	0.8034	1369.3044	0.2738	0.0657	649.8455
NiAlTiB (B)	10^{-4}	1073	4959.0670	1.1680	125.8930	0.0426	0.0382	109.5500
	10^{-3}	873	6520.7868	0.8217	1615.4741	0.2872	0.0735	763.2754

The compression tests conducted at room temperature showed small deformation of the A alloy (total elongation $\varepsilon \sim 0.175$). In the case of alloy B, for all initial strain rates ($\dot{\varepsilon}$) almost immediate failure of the samples after achieving certain stress level was observed. The value of maximal stress at which failure occurred is the higher the largest is $\dot{\varepsilon}$. Alloy A was observed to sustain larger strains, while the values of stress are smaller than in the case of alloy B. At higher temperatures, a gradual increase of deformation of both alloys was noted. Besides, the samples did not undergo cracking. The analogous behavior was also observed when the strain rate was changed. Thus, the brittle-ductile transition temperature was defined to be about 673 K and depended on titanium content.

Characteristics presented in a 3-axis coordinate system allowed us to conduct analysis of the dependence of strain in the function of temperature and strain rate. In Figures 4a and b, the dependencies are presented for both alloys in coordination system σ-ε-T and initial strain rate ($\dot{\varepsilon}$) = $1.85 \cdot 10^{-4}$ s^{-1}, which additionally confirms our earlier discussion. On the other hand, Figure 4c presents dependence σ-ε-$\dot{\varepsilon}$ at a constant temperature of 873 K for alloy A in the coordinate system σ-ε-$\dot{\varepsilon}$. No anomalies as those in the alloys with Ni_3Al matrix have been detected. It is also noted that, for higher initial strain rates, higher stresses are recorded (which is additionally confirmed by yield points collected in Table 2). Besides, the results of Vickers hardness HV10 (load 98.07 N) are also listed Table 2). An increase of yield point (at analogous deformation conditions) and

hardness HV10 by almost 7% is observed for alloys with higher titanium content (B alloy). The results for the A alloy were discussed in detail in [16]. The yield point decreases gradually with an increase of temperature until a significant drop is observed at 1073 K (Fig. 4, Tab. 2).

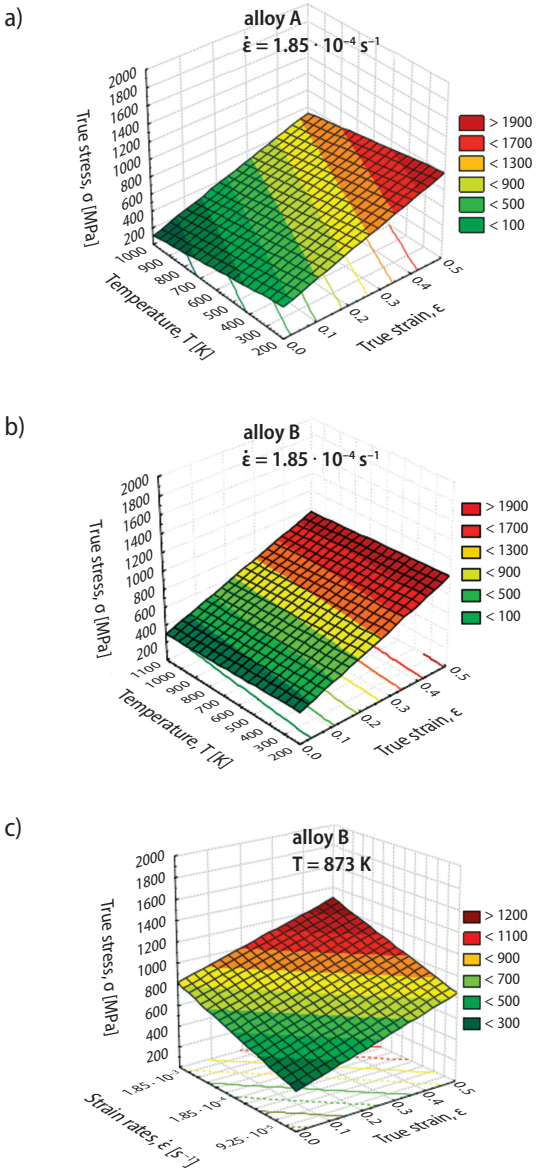

Fig. 4. Deformation characteristics of NiAlTiB alloys in a function of: a) σ-ε-T alloy A, $\dot{\varepsilon} = 1.85 \cdot 10^{-4}\ s^{-1}$; b) σ-ε-T alloy B, $\dot{\varepsilon} = 1.85 \cdot 10^{-4}\ s^{-1}$; c) σ-ε-$\dot{\varepsilon}$ alloy B, T = 873 K

In Figure 5, chosen logσ = f (logε) characteristics of alloys A and B are presented, while in Table 3, Hollomon coefficients describing various ranges (K_1, K_2, n_1, n_2) and border between ranges ($\varepsilon_{1/2}$, $\sigma_{1/2}$) are compiled.

Differences in strength coefficients (K) and hardening exponents (n) for a certain range of hardening depending on test temperature in NiAlTiB alloys (both A and B) were noted. Moreover, higher values of strength coefficients and hardening exponents at a given temperature for the first range of hardening in relation to their equivalents in the second range were observed. Additionally, in most cases, K_2 and n_2 decreased as temperatures increase.

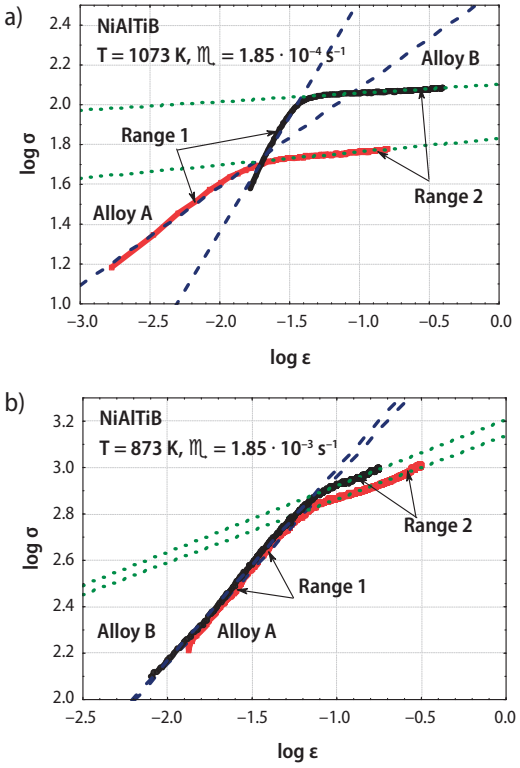

Fig. 5. Characteristics of dependencies log σ = f (logε) for both NiAlTiB alloys

Applying point, linear (Fig. 6) and surface (Fig. 7) analyses by means of the EDS method, it was possible to locate various phases (including that of NiAl). The precipitates present at the grain boundaries as well as inside grains of both types of alloys were identified to be enriched in titanium and boron. Distribution of these regions is inhomogeneous, which is reflected in mappings (Figs 6 and 7). Based on the performed analyses and structure observations, it should be also stated that prolonged annealing at 1523 K is insufficient for the complete homogenization of the alloys.

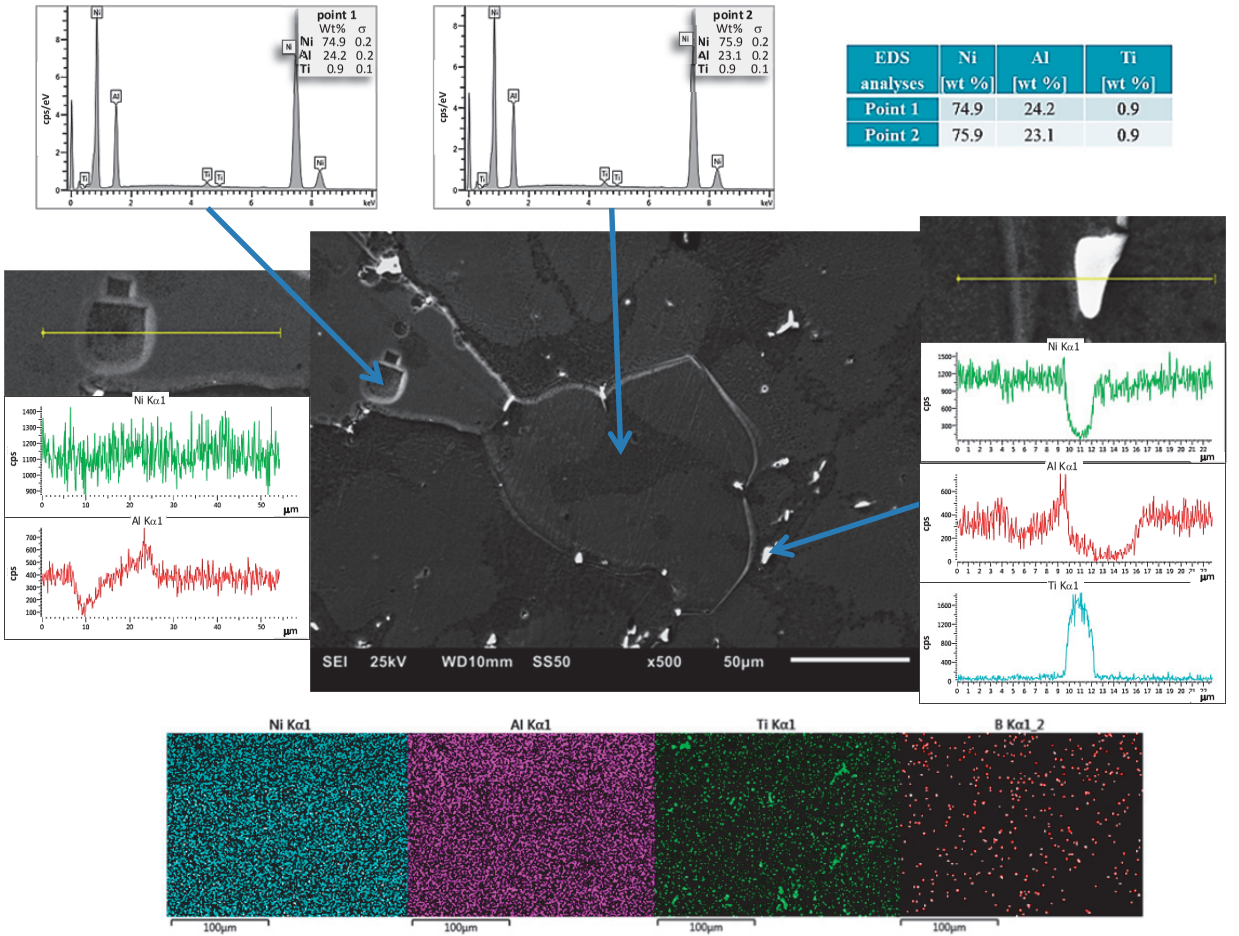

EDS analyses	Ni [wt %]	Al [wt %]	Ti [wt %]
Point 1	74.9	24.2	0.9
Point 2	75.9	23.1	0.9

Fig. 6. Microstructural observations of type A alloy by scanning electron microscope with included EDS analysis

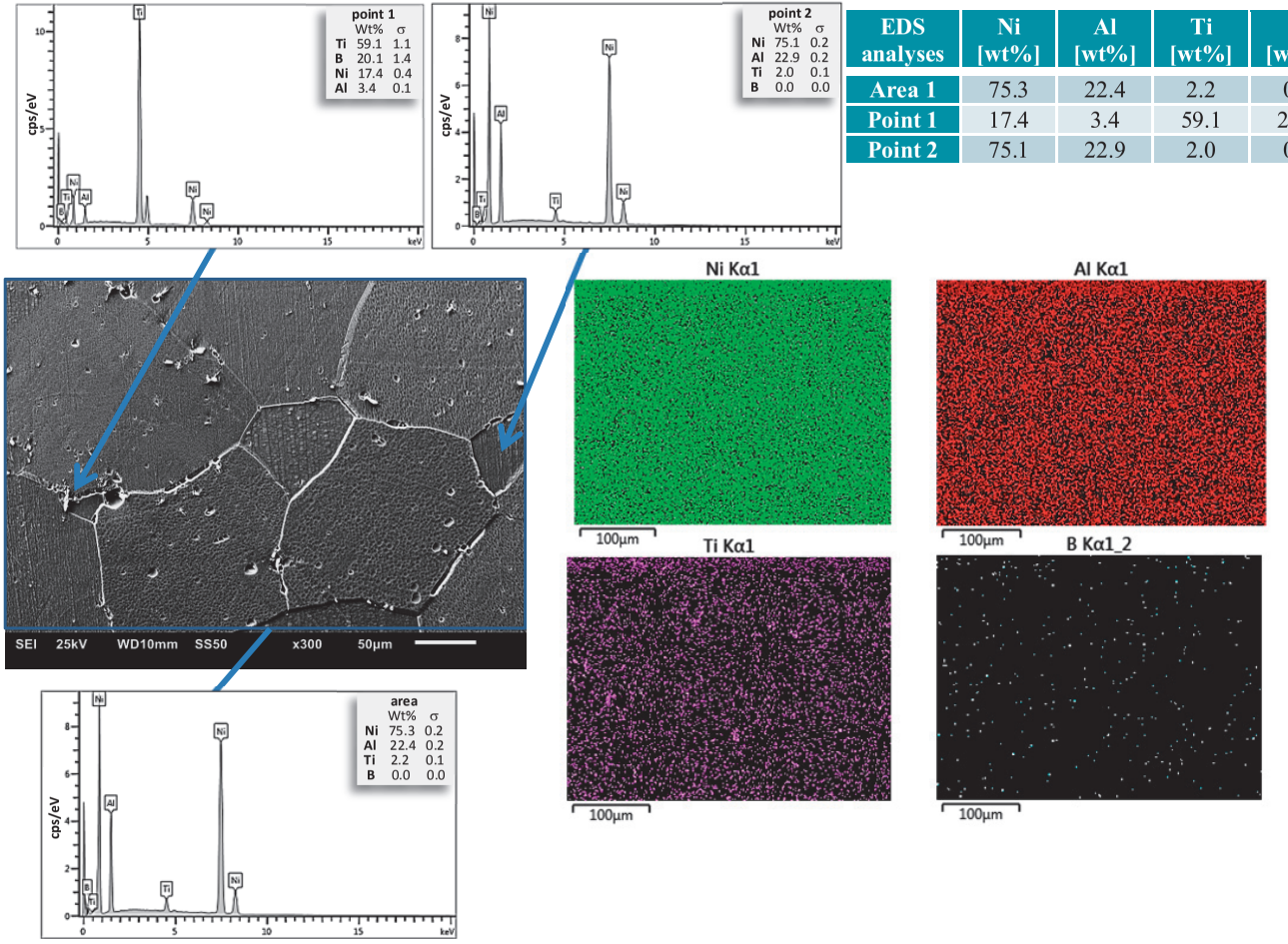

EDS analyses	Ni [wt%]	Al [wt%]	Ti [wt%]	B [wt%]
Area 1	75.3	22.4	2.2	0.0
Point 1	17.4	3.4	59.1	20.1
Point 2	75.1	22.9	2.0	0.0

Fig. 7. Microstructural observations of type B alloy by scanning electron microscope with included EDS analysis

As a result of the performed observations at different levels of deformation, it was found that cracking usually begins at grain boundaries in the case of alloy A (Fig. 8a) and later in regions enriched only by titanium or both titanium and boron (Fig. 8b). Further deformation lead to the inevitable failure of a sample. The before-failure microstructures of alloy A deformed at room temperature ($\varepsilon = 0.15$) and at 673 K ($\varepsilon = 0.17$) are shown in Figures 8b and 8c, respectively.

In the case of alloy B deformed at room temperature, a transcrystalline mechanism of cracking (Figs 9 and 10) was observed.

Similarly, the before-failure microstructures of alloy B deformed at 673 K ($\varepsilon = 0.07$) is shown in Figure 11.

Fractures characteristic of brittle failure of the samples deformed at temperatures of 297 K and 673 K for alloy A and B, respectively, are presented in Figure 12. Samples made of alloy B and deformed at room temperature encountered complete damage. On the other hand, samples of both alloys deformed at temperatures of 873 K and 1073 K, respectively, deformed without failure.

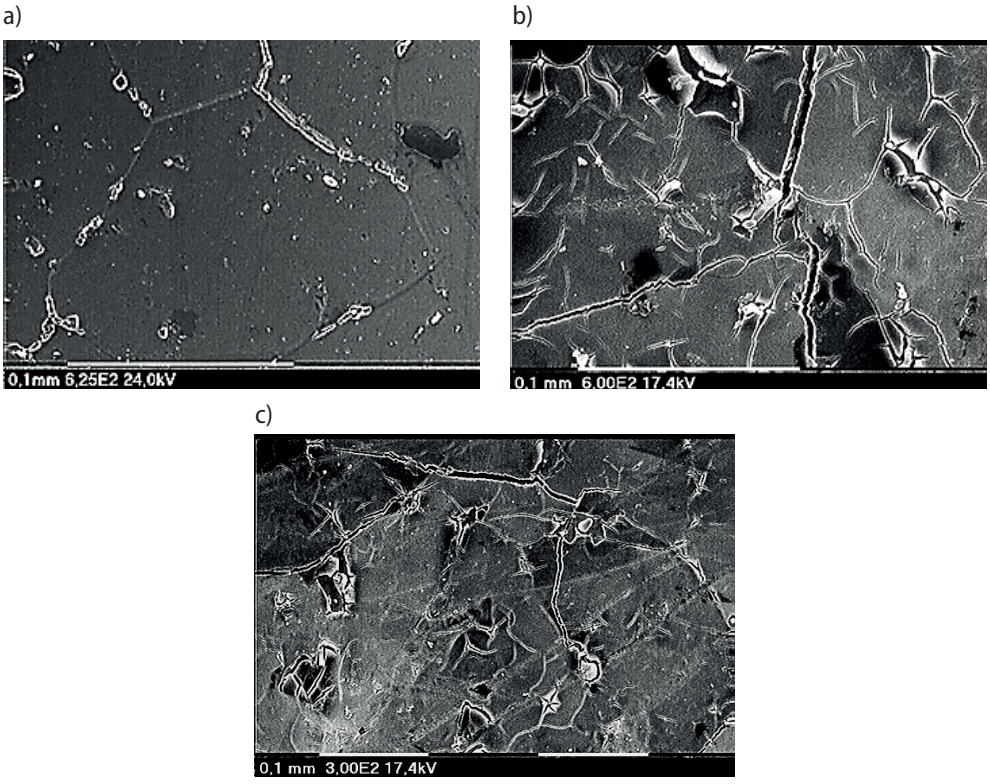

Fig. 8. Microstructural observations of type A of NiAlTiB alloy by scanning electron microscope: a) room temperature, $\varepsilon = 0.005$; b) room temperature, $\varepsilon = 0.15$; c) temperature of 673 K, $\varepsilon = 0.17$

a) b)

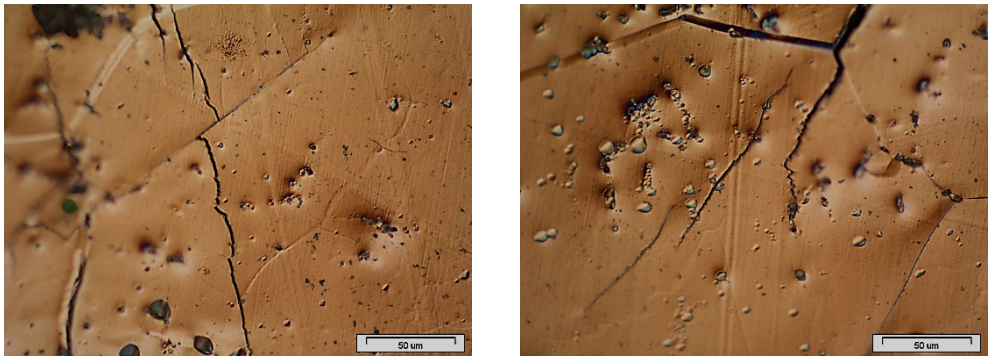

Fig. 9. Microstructural observations of type B of NiAlTiB alloy by optical microscope, room temperature, ε = 0.005

a) b)

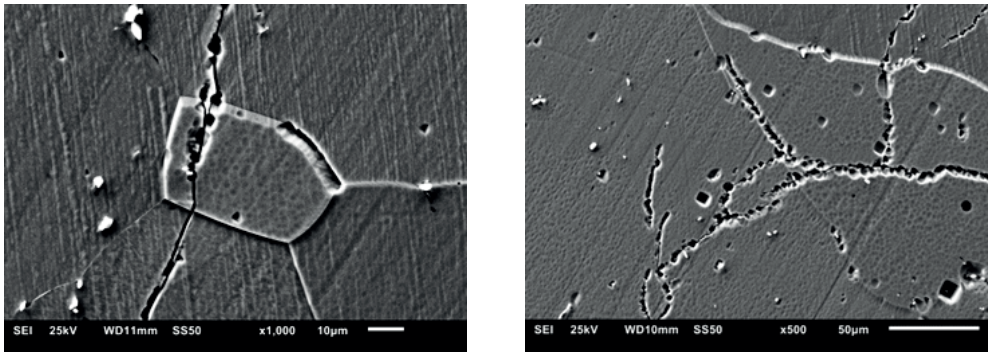

Fig. 10. Microstructural observations of type B of NiAlTiB alloy by scanning electron microscope, room temperature, ε = 0.005

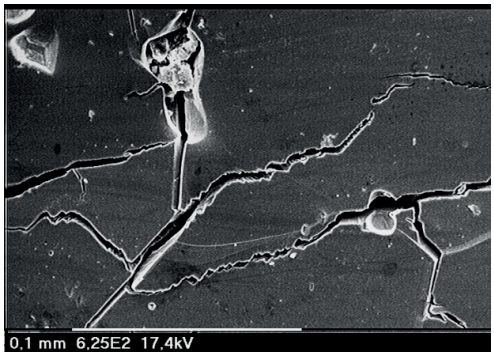

Fig. 11. Microstructural observations of type B of NiAlTiB alloy by scanning electron microscope, temperature of 673 K, ε = 0.07

a)

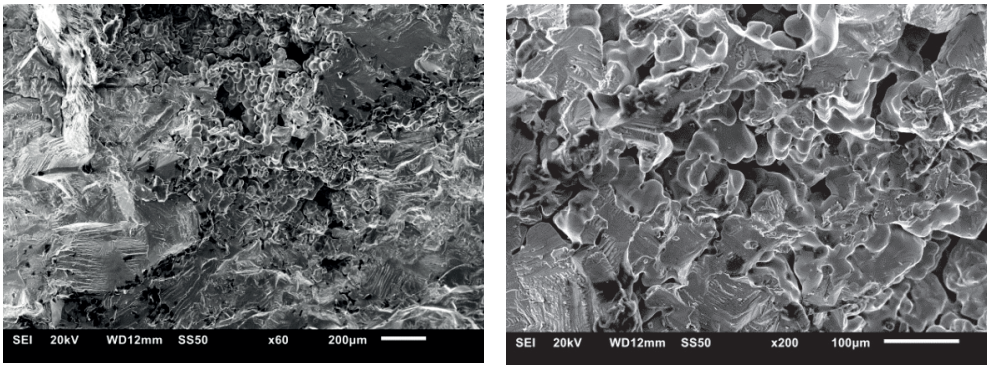

b)

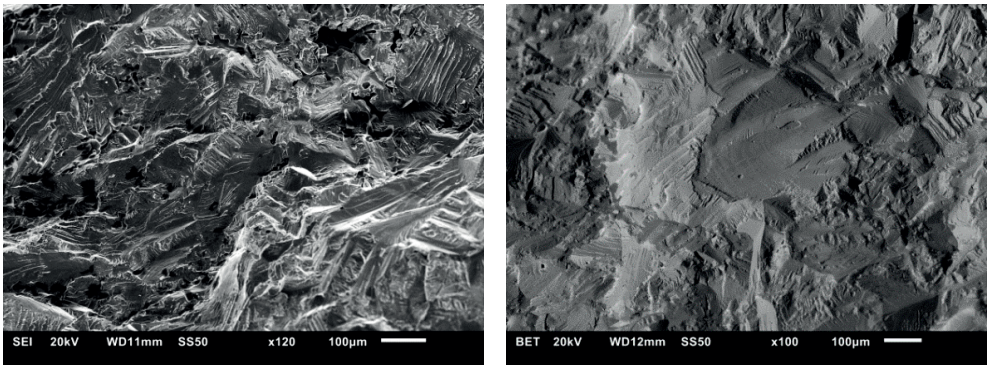

Fig. 12. Fracture micrographs of NiAlTiB alloys: a) alloy A deformed at 297 K; b) alloy B deformed at 673 K

3.2. Resistance to corrosion in NiAlTiB alloys

In Figure 13, corrosion potentials of NiAlTiB alloys appear to reach a constant value after 500 s. Values of the corrosion potentials of the samples are equal to -0.262 and 0.254 V for alloy A and B, respectively. In order to determine corrosion resistance of the alloys, voltammetric curves were prepared in a 1-mol solution of sulfuric acid, which are presented in Figure 14. The polarization curves of alloys containing titanium exhibit the presence of a small peak of active solubilizing at potential about 0V with respect to the Ag/AgCl electrode. Maximal current of the peak for both alloys is 2 mA/cm^2; then, it decreases and keeps a constant value at a wide range of potentials. The peak of active solubilizing is connected with the formation of a layer of corrosion products made from a mixture of nickel and aluminium oxides, which block the surface of the alloy. The presence of titanium significantly prohibits anodic solubilization of the alloy (small peak at polarization curve). The value of the corrosion potential of both alloys proves that the alloy is not subjected to active solubilization. E_{kor} reaches a value of potential in the region before active solubilization.

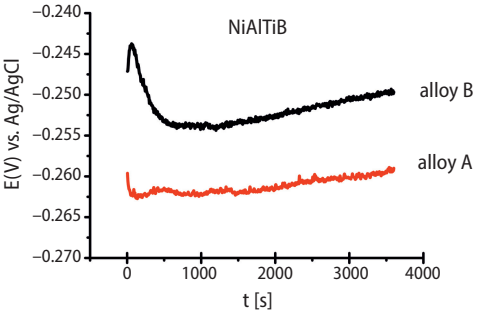

Fig. 13. Corrosion potential of NiAlTiB alloys measured in 1M H_2SO_4 solution

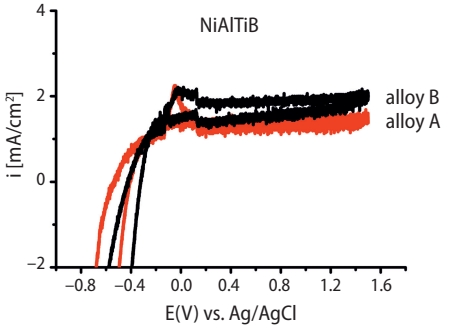

Fig. 14. Voltammetric curves for NiAlTiB alloy A and B with potential rate of 1V/min in 1M H_2SO_4 solution

A characteristic feature is the lack of peaks of cathodic reduction at the backward curve. Such behavior suggests that anodic solubilization of the alloy and the formation of corrosion products is an irreversible process.

4. Conclusions

It is possible to produce alloys on the basis of the NiAl matrix by means of the Exomelt cost-saving process. The obtained alloys are characterized by compact structure with homogeneously distributed regions enriched in titanium. Due to the application of this method, it becomes possible to shorten the production time of the alloy; thus, saving about 40% of energy.

The addition of titanium and boron causes embrittlement at room temperature; however, it influenced the improvement of mechanical properties at higher temperatures. At a temperature of 673 K or higher, it has been shown to increase plasticity, and the addition of titanium and boron resulted in an increase of strength. At temperatures of 873 and 1073 K, there was no destruction of samples in the compression test. Alloying additions resulted in an increase in hardness.

The conducted electrochemical studies of corrosion resistance of NiAlTiB alloys show that they undergo active solubilizing followed by the formation of a layer of corrosion products. The mentioned process is irreversible due to the lack of cathodic reduction peaks on the backward curve. The alloying addition remarkably influences corrosion resistance of Ni-Al alloys; e.g., alloys containing Ti are resistant to corrosion in sulfuric acid. Titanium oxide forming at the surface protects the alloy from active solubilizing.

Acknowledgements

This work was carried out with financial support through statutory funds of Pedagogical University in Krakow.

References

[1] Darolia R.: NiAl Alloys for high-temperature structural applications. JOM 43, 3 (1991), 44–49
[2] Trinh D., Műller M.: Aluminides, 4H1609 Functional Materials, Project report, KTH 2002
[3] Frommeyer G., Rablbauer R.: High Temperature Materials Based on the Intermetallic Compound NiAl Reinforced by Refractory Metals for Advanced Energy Conversion Technologies, Materials Technology. Steel Research International, 79, 7 (2008), 507–513
[4] Bojar Z., Przetakiewicz W. (red.): Materiały metalowe z udziałem faz międzymetalicznych. Wydawnictwo BEL Studio, Warszawa, 2006
[5] Noebe R.D., Bowman R.R., Nathal M.V.: The Physical and Mechanical Metallurgy of NiAl. Physical Metallurgy and Processing of Intermetallic Compounds, 1996, 212–296
[6] Hawk J.A., Alman D.E.: Abrasive wear behaviour of NiAl and NiAl-TiB_2 composites. Wear, 225–229 (1999), 544–556
[7] Colin J., Serna S., Campillo B., Flores O., Juárez-Islas J.: Microstructural and lattice parameter study of as-cast and rapidly solidified NiAl intermetallic alloys with Cu additions. Intermetallics, 16, 7 (2008), 847–853
[8] Zhou J., Guo J.T.: Effect of Ag alloying on microstructure, mechanical and electrical properties of NiAl intermetallic compound. Materials Science and Engineering A, 339 (2003), 166–174
[9] Hyjek P., Sulima I., Figiel P.: NiAl composite reinforced TiB_2 ceramic particles. In: M. Szutkowska (ed.), Innovative Manufacturing Technology 2013, The Institute of Advanced Manufacturing Technology, Krakow 2013, 31–42
[10] Shi-xiang Hou, Zong-de Liu, Dong-yu Liu: The study of NiAl-TiB2 coatings prepared by electro-thermal explosion ultrahigh speed spraying technology. Surface & Coatings Technology, 205 (2011), 4562–4568
[11] Hyjek P., Kurtyka P., Wierzbiński S., Krawiec H.: Odporność korozyjna kompozytów na osnowie stopu Al-Zn-Mg wzmacnianych cząstkami Al_2O_3, Kompozyty, 5, 2 (2005), 43–46
[12] Białobrzeski A., Czekaj E., Heller M.: Corrosive behaviour of aluminium and magnesium alloys processed by die casting technology. Archives of Foundry, 2, 3 (2002), 294–313
[13] Kmita A., Janas A., Hutera B.: Synthesis and evaluation of the structure of Ni_3Al/C alloy. Metallurgy and Foundry Engineering, 35, 2 (2009), 147–154
[14] Krupkowski A.: The deformation of plastic metals by strain. Annales de l'Académie Polonaise des Sciences Techniques, 7 (1946), 113–118
[15] Ludwigson D.C.: Modified stress-strain relation for FCC metals and alloys. Metallurgical Transactions, 2 (1971), 2825–2828
[16] Hyjek P., Sulima I.: Microstructure and mechanical properties of Ni-Al-Ti-B alloy. Ores and Non-Ferrous Metals, 60, 5(2015), 211–217